This is the accepted manuscript made available via CHORUS. The article has been published as:

Observation of Robust Zero-Energy Extended States

Jannatul Ferdous, Cem Yuce, Andrea Alù, and Hamidreza Ramezani

Phys. Rev. Applied **19**, L061002 — Published 23 June 2023

DOI: 10.1103/PhysRevApplied.19.L061002

Observation of Robust Zero Energy Extended States

Jannatul Ferdous[1], Cem Yuce[2], Andrea Alù[3,4], Hamidreza Ramezani[1*]
[1] *Department of Physics and Astronomy, University of Texas Rio Grande Valley, Edinburg, TX 78539, USA*
[2] *Department of Physics, Eskisehir Technical University, Eskisehir, Turkey*
[3] *Photonics Initiative, Advanced Science Research Center, City University of New York, New York, NY, 10031, USA*
[4] *Physics Program, Graduate Center, City University of New York, New York, NY, 10016, USA*

Topological edge states arise at the interface of two topologically-distinct structures and have two distinct features: they are localized and robust against symmetry protecting disorder. On the other hand, conventional transport in one dimension is associated with extended states, which typically do not have topological robustness. In this paper, using lossy coupled resonators in one dimension, we demonstrate both theoretically and experimentally the existence of robust states residing in the bulk. We show that they are unusually robust against disorders in coupling between adjacent sites and losses. Our work paves the way to a different form of robust transport that is not limited to boundary phenomena and can be accessed more easily from far field.

PACS numbers:

Introduction– The understanding of topological properties of meta-structures and their consequence in wave matter interaction has enormously expanded over the last decade, see [1] and references in it. One of the most practically relevant aspects of Hermitian topological systems is the existence of eigenstates with unusual protection against disorder. This is a direct consequence of the bulk boundary correspondence, based on which interfaces between bulk materials with different topological invariants necessarily support the presence of confined, highly robust states. In one dimensional systems, this phenomenon corresponds to the presence of a midgap state localized at the interface of two periodic linear arrays, one with nontrivial topology and the other one with trivial topology [2]. In 2D, a topological edge state with broken time reversal symmetry allows for edge transport immune to backscattering [3, 4]. In both 1D and 2D, edge states are exponentially localized at the interface.

The interest in topological states is not limited to Hermitian systems and it has been extended to non-Hermitian lattices [5–11]. This nontrivial extension was inspired by the associated exotic phenomena, and applications observed in open quantum and classical systems with gain and loss [12, 13]. In particular, non-Hermiticity removes the orthogonality of eigenstates and can therefore support a phase space with exceptional point singularities in which two or more eigenstates and their corresponding eigenvalues collapse to one eigenstate with one eigenvalue [15, 16]. Bi-orthogonality and the collapse of Hilbert space under these conditions lead to unconventional dynamical properties, including unidirectional invisibility [17], non-diffracting states [18], constant intensity waves [19], flat bands[20], unconventional lasing and absorption[21–24], ultra-fast state transfer[25–27], mode switching[28, 29], coherent perfect absorbers[30, 31], unidirectional wave manipulation[32, 34], non-reciprocal topological edge state [33], and anomalous phase transition [35], to name a few.

In topological systems, on the other hand, non-Hermiticity makes it possible to go beyond Bloch band theory and observe topologically robust lasers [36, 37], non-Hermitian skin effect [38–40], robust exceptional points [41, 42], topologically protected exceptional points [43], complex-energy braiding [44, 45].

The common theme in both Hermitian and non-Hermitian topological states is localization. The topological eigenstate remains localized when a transition occurs from one topological system to another one with different topology, avoiding radiation into the bulk. On the other hand, bulk states are extended all over space and thus are more fragile to disorder. This problem becomes more drastic when unavoidable non-Hermitian disorder is present, in the form of nonuniformly distributed loss originated from intrinsic material properties or radiation from the structure. Errors in fabrication can affect both intrinsic and radiation losses. While uniform loss can be analyzed using an exponential decay term, disordered non-uniform loss can generate nontrivial scattering responses [46, 47]. These non-trivial scattering features can be due to resonances solely associated with the non-Hermitian part of the potential and changes in the band diagram of the lattice. Consequently, it can be of great interest to search for nontrivial extended states that are immune to both disorder in Hermitian couplings and non-Hermitian terms in the potential (loss or gain), leading to robust diffraction management.

In this paper, using coupled resonators we propose and experimentally demonstrate the realization of a robust extended state corresponding to a zero mode originating from the deformation of a topological structure through changing the coupling constants and closing the gap. At first glance, it seems that such a deformation of the lattice causes the bulk boundary correspondence not to be directly applicable to explain the emergence of this robust bulk state. However, we show that due to the deformation in the lattice a zero-mode protected by the

symmetry intrudes into the band and consequently becomes de-localized while keeping its robustness. Here, we show theoretically and experimentally that such a robust extended state has resilience against disorder in both Hermitian coupling and non-Hermitian onsite potential. While for our experimental demonstration we use a phononic lattice, a similar phenomenon can be expected to emerge in photonic systems.

Theoretical analysis– While we will consider in the next section an acoustic waveguide system in a scattering setup to experimentally demonstrate topologically robust bulk states, we start our theoretical analysis with a non-Hermitian variant of the Su-Schrieffer-Heeger (SSH) model[48] with a nonuniform onsite loss or gain and with open boundary condition. This simple model can predict the physics of our experimental setup [49–51] and it can be easily adapted to photonic or electronic systems [52, 53]. The corresponding eigenvalue equation associated with our SSH system, namely $\mathcal{H}|\psi\rangle = \mathcal{E}|\psi\rangle$, in its spatial representation can be written as

$$\mathcal{E}\psi_j = t_{j-1}\psi_{j-1} + t_j\psi_{j+1} + i\gamma_j\psi_j, \quad \psi_0 = \psi_{N+1} = 0 \quad (1)$$

where $j = 1, 2, 3, ..., N$, with N being an odd number, and $t_j = \begin{cases} k & \text{if } j \text{ is odd} \\ c & \text{if } j \text{ is even} \end{cases}$. Here, k and c are staggering couplings along the lattice and we assume that $c \leq k$ are both real parameters. Furthermore, γ_j indicates the strength of loss ($\gamma_j < 0$) or gain ($\gamma_j > 0$) in each site.

The Hermitian SSH model with $\gamma_j = 0$ supports a bandgap in its spectrum equal to $2|k - c|$. Due to the chiral symmetry, the corresponding energy eigenvalues come in pairs, namely $\mathcal{E} = \pm E$. This guarantees that zero energy mode appears in the middle of the band gap when N is an odd number. In this case, the eigenmode associated with the zero energy eigenvalue is localized at one edge (here at right side) and its localization length increases as $|k - c| \to 0$ [54, 55]. Thus, the zero mode eigenstate becomes extended when the band gap vanishes at $k = c$. Both localized and extended zero energy modes are robust against coupling disorder, since the chiral symmetry remains intact in the presence of disorder in the couplings.

We can find the exact form of the extended zero mode at $k = c$ from Eq.(1)

$$\begin{cases} \psi_{2j-1} = \psi_1 & j = 1, 3, 5, ... \\ \psi_{2j+1} = -\psi_1 & j = 1, 3, 5, ... \\ \psi_{2j} = 0 & j = 1, 2, 3, 4, ... \end{cases} \quad (2)$$

The zero amplitude in the even sites is a consequence of the π phase difference between the nearest neighbors of each even site, which results in a destructive interference at the even sites. From Eq.(2) it is clear that the amplitude of the eigenmode associated with the zero mode is equally distributed at the odd sites, while it has zero amplitude on the even sites. Consequently, one can transfer

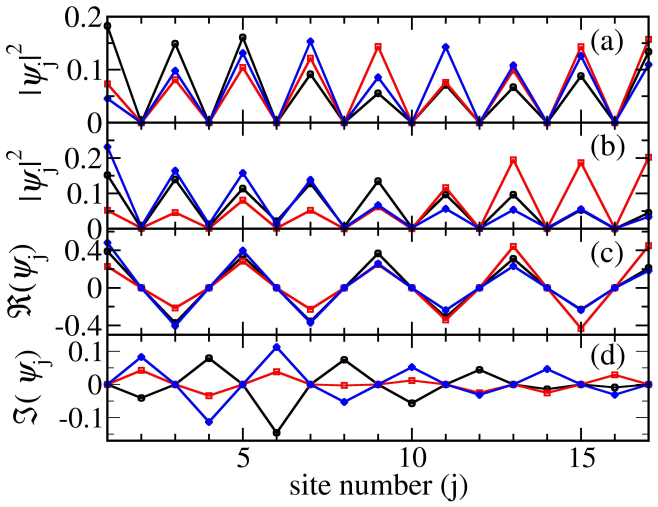


FIG. 1: (a) Mode profiles associated with the bulk zero mode in a system described by Hamiltonian $\mathcal{H}$ and gain, loss values given by Eq.(3) with 20% disorder in the couplings and $\gamma = 0.2$. The couplings without disorder are chosen such that $k = 1, c = 0.5$. For all realizations the zero mode remains zero in its real part while its imaginary part is equal to 0.2. (b) The same as (a) but this time γ_j is selected randomly from a uniform distribution $[-0.2, 0.2]$. We observe that the intensity at even sites is no longer zero. In (c,d) we plot the real and imaginary parts of the curves in (b). We observe that odd sites are purely real and even sites are purely imaginary, confirming the π phase shift among odd sites.

a localized edge state in the Hermitian SSH model to an extended bulk state by deformation of the lattice by means of making $k = c$, while preserving its robustness.

Now let us discuss the addition of non-Hermitian terms $\gamma_j \neq 0$ in Eq.(1) when $k = c$. To begin with, let us consider the Hermitian, H_0 and non-Hermitian H_I parts of the Hamiltonian associated with our model, $\mathcal{H}$. Specifically, $\mathcal{H}$ would be an $N \times N$ matrix that its only non-zero elements are $\mathcal{H}_{j,j+1} = \mathcal{H}_{j+1,j} = k$ and $\mathcal{H}_{j,j} = i\gamma_j$. we can show that for

$$\gamma_j = (-1)^j\gamma, \quad j = 1, 2, 3, ... \quad (3)$$

we have $\{H_0, H_I\} = 0$. The last relation implies that the two Hamiltonians H_0 and H_I anti-commute with each other. This anti-commutation condition corresponds to the *chiral symmetry* condition for H_0. In other words, under constraint (3), the non-Hermitian Hamiltonian H_I can be considered as the chiral symmetry operator for the Hamiltonian H_0. However, the total Hamiltonian $\mathcal{H}$ is not chiral symmetric. A consequence of the anti-commutation is that H_0 and H_I share a common energy eigenstate. It turns out that this common eigenstate is the zero energy eigenstate of H_0 with eigenvalue $-i\gamma$, as it satisfies the aforementioned chiral symmetry. We keep calling this purely imaginary mode the zero mode, since its real part is still zero. This is a unique feature of the zero eigenmode, and there exists no such other eigenstate

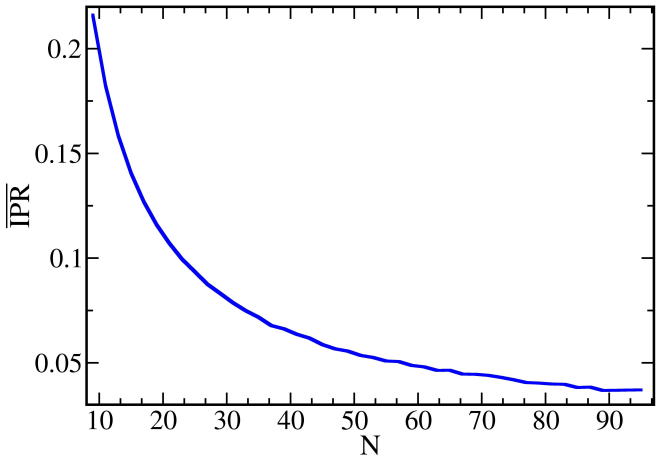


FIG. 2: Average inverse participation ratio, $\overline{IPR}$, associated with the zero mode as a function of N. For each realization we added 20% and 10% disorder to the couplings and imaginary onsite potential, respectively. The existence of the $1/N$ behavior depicts that the zero mode remains extended in the present of disorder.

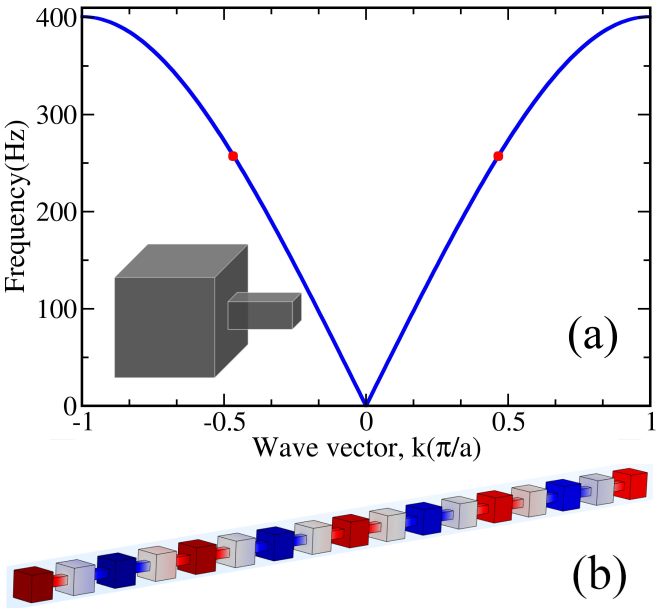


FIG. 3: (a) Band-structure for the periodic acoustic waveguide whose unit cell is shown in the inset. The frequency associated with the robust bulk state is identified with red dots on the band diagram. The unit cell is composed of cuboids with dimension $7 \times 7 \times 7$ cm^3 connected to a rectangle with dimension $2.3 \times 2.3 \times 7$ cm^3. Our waveguide system is made of such 17 cuboids connected by 16 rectangles. (b) Mode profile of the robust extended mode of the waveguide composed of 17 cuboids around eigenfrequency 257 Hz.

that is shared between H_0 and H_I.

In the presence of disorder in the couplings, the anti-commutation relation is still preserved, and thus the common zero mode eigenvector remains intact. In this case, the real and imaginary parts of the zero mode associated with $\mathcal{H}$ remain intact, and the only quantity that changes is the eigenvector associated with the zero mode. Particularly, we no longer have a uniform eigenvector for the zero mode of $\mathcal{H}$. In other words, while we have $\psi_{2j} = 0$ as in Eq.(2), we will not have $|\psi_{2j+1}| = |\psi_1|$. We have plotted the amplitude at each site associated with the zero mode eigenvalue in Fig.(1a) for different strengths of disorder in the couplings, which confirms our last statement. Notice that, even for very strong disorder in the coupling we obtain the zero mode, but there is a possibility of having the mode localized and no longer distributed in the bulk.

So far it appears that $\psi_{2j} = 0$ is the signature of the zero mode independent of the presence of disorder in the couplings and of constraint (3) on H_I. We introduce now an imaginary part to disorder in the diagonal elements of H_I, while we keep the disorder in the coupling elements of H_0. By adding such disorder to H_I, namely randomly choosing γ_j from a uniform distribution, the anti-commutation relation between H_0 and H_I will not be valid anymore. This is also expected when we consider scattering from a multi-layered medium, since both the imaginary and real parts of the index of refraction play a role in the scattering process. We do not expect that, in the presence of pure imaginary onsite disorder, the zero mode and its corresponding bulk state remain intact. However, our numerical simulations show that the zero mode still has a zero real part, and only its imaginary part is affected by non-Hermitian disorder. To explain this effect, we can use non-degenerate first-order perturbation theory, based on which to first-order approximation the shift in the zero mode eigenvalue is given by

$$E_0^{(1)} = i \left\langle 0^{(0)} \middle| H_I \middle| 0^{(0)} \right\rangle \tag{4}$$

in which $\left|0^{(0)}\right\rangle$ is the eigenvector associated with the zero mode energy of H_0 in the presence of disorder in the couplings. Clearly, $E_0^{(1)}$ in Eq.(4) is purely imaginary, and thus the disorder in the imaginary part of the onsite potentials does not change the real part of the zero mode. This means that the bulk zero mode is robust against disorder in the couplings and its real part is also robust against onsite purely imaginary disorder.

To further show that, in the presence of disorder in couplings, as well as of an onsite imaginary potential, the zero mode remains as extended state in Fig. 2, we have plotted the average inverse participation ratio, $\overline{IPR} = \frac{\sum_{j=0}^{j=N} |\psi_j|^4}{R(\sum_{j=0}^{j=N} |\psi_j|^2)^2}$, as a function of system size N for the zero mode in which R is the number realizations. The inverse participation ratio must evolve as $\frac{1}{N}$ for an extended state [57]. To be more specific, in our numerical calculations we added 20% disorder into the couplings and 10% disorder in the imaginary part of the onsite potentials in our tight-binding model and calculated $\overline{IPR}$

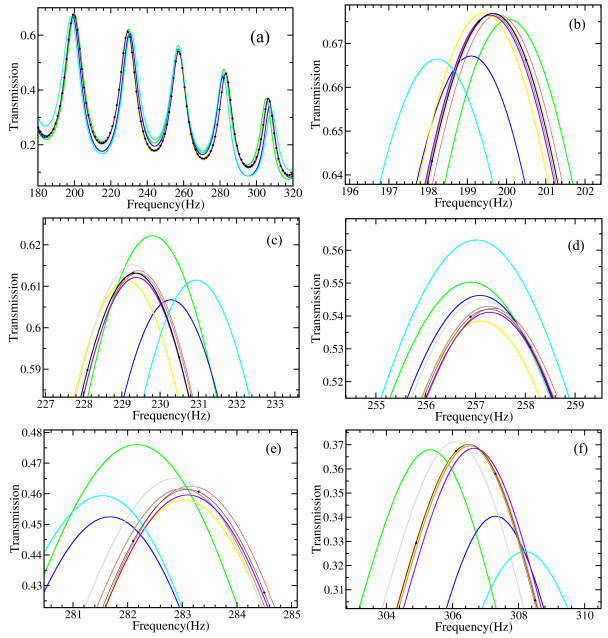


FIG. 4: (a) Full-wave numerical demonstration of topologically protected robust bulk state depicting transmission as a function of frequency for the different realization of the acoustic waveguide in Fig.(3). The black line with diamond symbols is associated with the waveguide with no disorder. The other lines are associated with different disorders. The robust mode occurs at frequency ≈ 257 Hz. (b-f) We have zoomed around the resonances to better show how each peak is shifted for different realizations. We observe that the resonance associated with the robust bulk state in (d) has the least shift, ≈ 0.35 Hz while the other resonances have ≈ 1.5 Hz due to the disorder which is more than 4 times the shift of the robust bulk state undergoes.

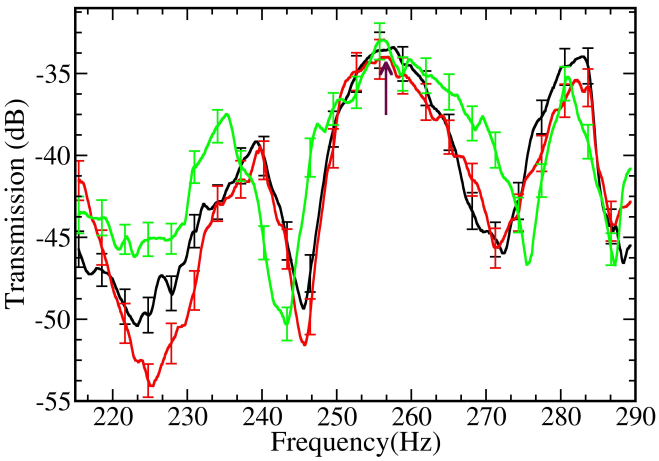


FIG. 5: Experimental verification of robust bulk state. The transmission spectrum for the system without disorder with uncontrolled small loss is displayed by the black curve, while the systems with disorder with uncontrolled loss are shown by the red and green curves. Resonance peaks are shown with stars. The robust bulk state is observed around 257 Hz indicated with an arrow which has the smallest shift.

over $R = 1000$ realizations. Qualitatively, in Fig. 2 we do observe that the $\overline{IPR}$ evolves as $1/N$.

The above results become more interesting when we consider the eigenvector associated with the zero mode in the presence of a purely imaginary onsite potential. More specifically, as it is depicted in Fig(1b), the eigenmode associated with the zero mode does not necessarily have zero intensity in every other site, meaning that $|\psi_{2j}| \neq 0$. Although $|\psi_{2j}| \neq 0$, as it is shown in Fig.(1c,d) the imaginary part of wave-function at odd sites is zero and thus it is always real while the even sites are always purely imaginary. This means that there is a $\frac{\pi}{2}$ phase difference between nearest-neighboring sites, and thus a π phase difference between the sites at odd positions. However, this π phase shift does not lead to destructive interference at even sites as now the wave function can be complex at different sites. Thus, we can conclude that the π phase shift between the adjacent odd sites is a signature of a robust bulk zero mode even if the mode is distributed all over the system in a non-uniform way.

Experimental observation of robust bulk state– To demonstrate the predicted robust bulk state experimentally, we use an airborne acoustic waveguide composed of coupled Helmholtz resonators in a scattering setup. As we show later, this waveguide system supports a bulk state with all the properties of the zero mode in the Hamiltonian in Eq.(1). Note that in the acoustic experimental setup, we can only leverage loss as non-Hermitian element. Yet, all previous discussions remain valid since the sign of γ does not play a role in our derivations. This is because addition of an offset loss will not change the physics.

The acoustic system considered here is a two-port hollow waveguide composed of 17 cuboids resonators with dimension $7 \times 7 \times 7$ cm^3 coupled to each other by rectangles with dimension $2.3 \times 2.3 \times 2.3$ cm^3. The fabricated sample is made of polystyrene foam sheets with density 1050 $\frac{\text{kg}}{\text{m}^3}$ and bulk modulus 16.5 MPa with an average thickness of 5 mm. The inner cross-section of the waveguide along the cuboids is kept at 49 cm^2 and along the rectangles is kept at 5.29 cm^2. A similar system has been used previously to generate a tunable non-Hermitian acoustic filter [56].

In the search for the robust bulk state, in Fig.(3a) we plotted the lowest band using numerical full-wave simulations, where we assumed the density of air $\rho = 1.4$ $\frac{\text{kg}}{\text{m}^3}$, while the effective bulk modulus $\beta = 0.931\times10^5(1+0.01i)$ Pa. The imaginary part of β describes the loss in our actual setup. Figure (3b) confirms that the mode at frequency ≈ 257 Hz, indicated with the stars in Fig.(3a), has a very similar form as the one described in Eq. (2), and thus we expect it to correspond to the robust bulk state at this frequency. To check this claim using full-wave simulation, in Fig. (4a) we plot the transmission associated with the scattering scenario where the system

is excited from the left and the signal is collected at the right port. Specifically, the black curve with diamond symbols is the transmission without disorder and uniform loss. The other curves correspond to the cases in which we added 10% random disorder to the couplings by changing the length of the cavity sides. We then compared the peaks at different frequencies. Clearly, as it is also shown in Fig.(4b-f), the peak associated with the frequency of $\approx$ 257 Hz undergoes maximum shift which is less than $\frac{1}{4}$ of the maximum shift that other peaks. It worth to mention that this acoustic model does not have chiral symmetry as the band disperses linearly at $\approx$ 257 Hz (zero frequency) and quadratic at the upper band edge.

The experimental data corresponding to the transmitted signal for a range of frequencies between 215 Hz and 290 Hz for three different samples are shown in Fig.(5). In our setup using a function generator, we send an acoustic continuous sinusoidal signal with fixed amplitude to different samples with disorder in the couplings. We measured the transmitted acoustic signal using $\frac{1}{4^{th}}$ omnidirectional microphones. We connected the microphones to the network analyzer via a constant current power supply to send a low-impedance signal to the network analyzer. We observed the spectrum of the transmitted acoustic wave in the network analyzer from where we extract our data. Specifically, in Fig.(5 the black curve corresponds to the transmitted signal for the almost perfect system without disorder with almost uniform loss induced by the leakage and absorption of sound through foam sheets along the structure. The red and green curves correspond to the transmitted signal for two different disordered systems where we added 10% disorders to the length of the couplings without moderating the loss. The black stars indicate the resonance peak frequencies in each sample. At the frequency of $\approx$ 257 Hz, the middle peak of Fig. (5), a smaller shift in the resonance peak is found in comparison to the other two peaks around 230 Hz and 280 Hz, demonstrating the inherent robustness of the bulk topological state.

To conclude, we have demonstrated the realization of a protected state against a disorder that belongs to the bulk and it is not necessarily localized to an edge. The robustness of the bulk state is not affected by coupling disorder and/or disorder in the imaginary part of the potential. While the bulk boundary correspondence cannot directly explain the robustness of the bulk state, the intrusion of the edge state into the band is responsible for the source of the robustness of the bulk state, and therefore the robustness has indirectly a topological origin. We believe that the demonstration of a topologically robust bulk state offers a different perspectives not only in phononics but also in photonics and other application fields. Our results provide a route for robust devices where robust excitation and transport of signals in the bulk is possible.

H.R. acknowledges the support by the Army Research Office Grant No. W911NF-20-1-0276, and NSF Grants No. PHY-2012172 and No. OMA-2231387. C. Y. acknowledge the support from the Scientific and Technological Research Council of Turkey through the 2219 program with grant number 1059B191900044. A. A. has been supported by the Air Force Office of Scientific Research and the Simons Foundation.

* Electronic address: hamidreza.ramezani@utrgv.edu

[1] H. Price, Y. Chong, A. Khanikaev, H. Schomerus, L. J. Maczewsky, M. Kremer, M. Heinrich, A. Szameit, O Zilberberg, Y. Yang, Roadmap on Topological Photonics, J. Phys. Photonics ,**4** 032501, (2022)

[2] L. Lu, J. D. Joannopoulos, and M. Soljacic, Topological photonics. Nature photonics, **8** (11), pp.821-829. (2014)

[3] A. B. Khanikaev, and G. Shvets, Two-dimensional topological photonics. Nature photonics, **11**(12), pp.763-773. (2017)

[4] M. Kim, Z. Jacob, & J. Rho, Recent advances in 2D, 3D and higher-order topological photonics. Light Sci Appl 9, 130 (2020).

[5] Hongfei Wang, Xiujuan Zhang, Jinguo Hua, Dangyuan Lei, Minghui Lu, and Yanfeng Chen, Topological physics of non-Hermitian optics and photonics: a review, J. Opt. **23** 123001 (2021)

[6] Henning Schomerus, "Topologically protected midgap states in complex photonic lattices," Opt. Lett. **38**, 1912-1914 (2013)

[7] C. Yuce, Topological phase in a non-Hermitian PT symmetric system, Phys. Lett. A **379**, 1213 (2015)

[8] S. Longhi, Topological phase transition in non-Hermitian quasicrystals, Physical review letters **122** (23), 237601 (2019)

[9] Mattis Reisner, Matthieu Bellec, Ulrich Kuhl, and Fabrice Mortessagne, "Microwave resonator lattices for topological photonics," Opt. Mater. Express **11**, 629-653 (2021)

[10] F. Mostafavi, C. Yuce, O. Magana-Loaiza, H. Schomerus, H. Ramezani, Robust localized zero-energy modes from locally embedded PT-symmetric defects, Physical Review Research **2** (3), 032057 (2020)

[11] H. Gao, H. Xue, Z. Gu, T. Liu, J. Zhu, B. Zhang, Non-Hermitian route to higher-order topology in an acoustic crystal, Nature communications **12** (1), 1-7 (2021)

[12] R. El-Ganainy, K. Makris, K., M. Khajavikhan, Ziad H. Musslimani, Stefan Rotter, and Demetrios N. Christodoulides , Non-Hermitian physics and PT symmetry. Nature Phys **14**, 11–19 (2018).

[13] Zhongming Gu, He Gao, Pei-Chao Cao, Tuo Liu, Xue-Feng Zhu, and Jie Zhu, Controlling Sound in Non-Hermitian Acoustic Systems, Phys. Rev. Applied **16**, 057001 (2021)

[14] C. Yuce, Robust bulk states, Physics Letters A, **383**, 15, 1791-1794, (2019)

[15] C. Shi, M. Dubois, Y. Chen, L. Cheng, H. Ramezani, Y. Wang, X. Zhang, Accessing the exceptional points of parity-time symmetric acoustics, Nature communications 7 (1), 1-5 (2016)

[16] M. A. Miri , A. Alu, Exceptional points in optics and photonics. Science, 363(6422):eaar7709 (2019)

[17] Zin Lin, Hamidreza Ramezani, Toni Eichelkraut, Tsampikos Kottos, Hui Cao, and Demetrios N. Christodoulides, Unidirectional Invisibility Induced by PT-Symmetric Periodic Structures, Phys. Rev. Lett. **106**, 213901 (2011)

[18] C. Yuce, H. Ramezani, Non-diffracting states at exceptional points, Optics Letters **46** (4), 765-768 (2021)

[19] M. Dehghani, C. Yuce, T. Kottos, H. Ramezani, Constant intensity conical diffraction in discrete one-dimensional lattices with charge-conjugation symmetry, Optics Letters **45** (1), 101-104 (2020)

[20] Hamidreza Ramezani, Non-Hermiticity-induced flat band, Physical review A **96**(1), 011802 (2017)

[21] L. Ge, YD. Chong, S. Rotter, HE. Tureci, A. D. Stone, Unconventional modes in lasers with spatially varying gain and loss, Physical Review A **84** (2), 023820 (2011)

[22] H. Ramezani, HK. Li, Y. Wang, X. Zhang, Unidirectional spectral singularities, Phys. Rev. Lett., **113** (26), 263905 (2014)

[23] Hamidreza Ramezani, Spectral singularities with directional sensitivity, Physical Review A **103** (4), 043516 (2021)

[24] H. Ramezani, Y. Wang, E. Yablonovitch, X. Zhang, IEEE Journal of Selected Topics in Quantum Electronics **22** (5), 115-120 (2016)

[25] B. T. Torosov, G. Della Valle, S. Longhi, Non-Hermitian shortcut to adiabaticity, Physical Review A **87** (5), 052502 (2013)

[26] F. Mostafavi, L. Yuan, H. Ramezani, Eigenstates Transition Without Undergoing an Adiabatic Process, Phys. Rev. Lett., **122** (5), 050404 (2019)

[27] Y.X. Shen, L.S. Zeng, Z.G. Geng, D.G. Zhao, Y.G. Peng, J. Zhu, X.F. Zhu, Acoustic topological adiabatic passage via a level crossing, SCIENCE CHINA Physics, Mechanics & Astronomy **64** (4), 1-8 (2021)

[28] J. Doppler, A. Mailybaev, J. Böhm, Ulrich Kuhl, A. Girschik, F. Libisch, T. J. Milburn, P. Rabl, N. Moiseyev, S. Rotter, Dynamically encircling an exceptional point for asymmetric mode switching. Nature **537**, 76–79 (2016)

[29] X. Shu, A Li, G. Hu, J. Wang, A. Alù, L. Chen, Fast encirclement of an exceptional point for highly efficient and compact chiral mode converters, Nature Communications **13** (1), 1-6

[30] D. Baranov, A. Krasnok, T. Shegai, A. Alù, Y. Chong. Coherent perfect absorbers: linear control of light with light. Nat. Rev. Mater. **2**, 17064 (2017).

[31] Z. Gu, T. Liu, H. Gao, S. Liang, S .An, J. Zhu, Acoustic coherent perfect absorber and laser modes via the non-Hermitian dopant in the zero index metamaterials, Journal of Applied Physics 129 (23), 234901 (2021)

[32] A. Farhi, A. Mekawy, A. Alù, D. Stone, Excitation of absorbing exceptional points in the time domain, Phys. Rev. A **106**, L031503 (2022)

[33] Mengyao Li, Xiang Ni, Matthew Weiner, Andrea Alù, and Alexander B. Khanikaev, Phys. Rev. B **100**, 045423 (2019)

[34] X. Wen, X. Zhu, A. Fan, W. Y. Tam, J. Zhu, H. W. Wu, F. Lemoult, M. Fink, J. Li, Unidirectional amplification with acoustic non-Hermitian space-time varying metamaterial. Commun Phys **5**, 18 (2022).

[35] L. Ge, Anomalous parity-time–symmetry transition away from an exceptional point, Physical Review A **94** (1), 013837 (2016)

[36] M. A. Bandres, S. Wittek, G. Harari, M. Parto, J. Ren, M. Segev, D. N. Christodoulides, M. Khajavikhan, "Topological insulator laser: Experiments." Science 359.6381 (2018).

[37] Yongquan Zeng, Udvas Chattopadhyay, Bofeng Zhu, Bo Qiang, Jinghao Li, Yuhao Jin, Lianhe Li, Alexander Giles Davies, Edmund Harold Linfield, Baile Zhang, et.al., Electrically pumped topological laser with valley edge modes. Nature 578, 246–250 (2020).

[38] Nobuyuki Okuma, Kohei Kawabata, Ken Shiozaki, and Masatoshi Sato, Topological origin of non-Hermitian skin effects. Physical review letters **124**, 8, 086801 (2020)

[39] Fei Song, Tao Shunyu, and Zhong Wang, Non-Hermitian skin effect and chiral damping in open quantum systems. Phys. Rev. Lett., **123**, 17, 170401 (2019): .

[40] S. Longhi, Probing non-Hermitian skin effect and non-Bloch phase transitions, Physical Review Research, 1(2), 023013 (2019)

[41] C. Yuce, & Hamidreza Ramezani, Robust exceptional points in disordered systems, EPL (Europhysics Letters) 126, 1 , 17002 (2019)

[42] J. D. Rivero, & L. Ge, Origin of robust exceptional points: Restricted bulk zero mode. Physical Review A, 101(6), 063823 (2020)

[43] Zhongming Gu, He Gao, Tuo Liu, Shanjun Liang, Shuowei An, Yong Li, and Jie Zhu, Topologically Protected Exceptional Point with Local Non-Hermitian Modulation in an Acoustic Crystal, Physical Review Applied **15**, 1, 014025 (2021)

[44] Kai Wang, Avik Dutt, Charles C. Wojcik & Shanhui Fan, Topological complex-energy braiding of non-Hermitian bands, Nature 598.7879 59-64 (2021)

[45] Haiping Hu, Sun Shikang , and Chen Shu, Knot Topology of Exceptional Point and Non-Hermitian No-Go Theorem, Phys. Rev. Research **4**, L022064 (2021).

[46] E. Rivet, A. Brandstötter, K. G. Makris, H. Lissek, S. Rotter & R. Fleury, Constant-pressure sound waves in non-Hermitian disordered media, Nature Physics **14**, 9 942-947 (2018)

[47] A. F. Tzortzakakis, K. G. Makris, and E. N. Economou, Non-Hermitian disorder in two-dimensional optical lattices, Physical Review B, **101**, 014202 (2020)

[48] W. P. Su, J. R. Schrieffer, and A. J. Heeger, Solitons in Polyacetylene, Phys. Rev. Lett., **42**, 1698 (1979).

[49] Xin Li; Yan Meng, Xiaoxiao Wu, Sheng Yan, Yingzhou Huang, Shuxia Wang, Weijia Wen, Su-Schrieffer-Heeger model inspired acoustic interface states and edge states, Applied Physics Letters, **113** 203501, (2018)

[50] Li-Yang Zheng, Vassos Achilleos, Olivier Richoux, Georgios Theocharis, and Vincent Pagneux, Observation of edge waves in a two-dimensional Su-Schrieffer-Heeger acoustic network, Physical Review Applied, **12**, 034014 (2019)

[51] Antonin Coutant, Audrey Sivadon, Liyang Zheng, Vassos Achilleos, Olivier Richoux, Georgios Theocharis, and Vincent Pagneux, Acoustic Su-Schrieffer-Heeger lattice: Direct mapping of acoustic waveguides to the Su-Schrieffer-Heeger model, Phys. Rev. B, 103, 224309 (2021)

[52] Alexander B. Khanikaev, Come to light, Nature Physics 13 6 532-533 (2017)

[53] Ching Hua Lee, Stefan Imhof, Christian Berger, Florian

Bayer, Johannes Brehm, Laurens W. Molenkamp, Tobias Kiessling & Ronny Thomale, Topolectrical Circuits, Commun Phys **1**, 39 (2018).

[54] J. K. Asbòth, L. Oroszlàny, and A. Pàlyi, A Short Course on Topological Insulators: Band Structure and Edge States in One and Two Dimensions, Lecture notes in physics 919,166, (2016)

[55] C. Yuce, Pseudo topological insulators, Phys. Let. A **383**, 248-251 (2019).

[56] S. Puri, J. Ferdous, A. Shakeri, A. Basiri, M. Dubois, and H. Ramezani, Tunable Non-Hermitian Acoustic Filter, Physical Review Applied **16**, 014012 (2021)

[57] Cem Yuce and Hamidreza Ramezani, Coexistence of extended and localized states in the one-dimensional non-Hermitian Anderson model, Phys. Rev. B **106**, 024202 (2022)